Research Square

Preprints are preliminary reports that have not undergone peer review.
They should not be considered conclusive, used to inform clinical practice,
or referenced by the media as validated information.

Inversion of thermal field-scale flow in porous media using conditional Karhunen-Loève expansion combined with Levenberg-Marquardt and Singular Value Decomposition schemes

Juarez dos Santos Azevedo

jdazevedo@ufba.br

Federal University of Bahia

Jarbas A. Fernandes

Federal University of Western Bahia

Marcus V. Americano da Costa

Federal University of Santa Catarina

Research Article

Keywords: Geothermal energy, Inverse problem, Conditional Karhunen-Loéve expansion

Posted Date: September 16th, 2026

DOI: https://doi.org/10.21203/rs.3.rs-7013832/v1

License: This work is licensed under a Creative Commons Attribution 4.0 International License.
Read Full License

Additional Declarations: No competing interests reported.

Inversion of thermal field-scale flow in porous media using conditional Karhunen-Loève expansion combined with Levenberg-Marquardt and Singular Value Decomposition schemes

Juarez dos Santos Azevedo[1*], Jarbas A. Fernandes[2] and Marcus V. Americano da Costa [3]

[1*], Institute of Science, Technology and Innovation, Federal University of Bahia, Camaçari-BA, 42802-721, Brazil.
[2]Multidisciplinary Center, Federal University of Western Bahia, Bom Jesus da Lapa-BA, 47600-000, Brazil.
[3]National Institute of Science and Technology in Control and Automation of Energy Processes, Department of Automation and Systems Engineering, Federal University of Santa Catarina, Florianópolis-SC, 88040-900, Brazil.

*Corresponding author(s). E-mail(s): jdazevedo@ufba.br;
Contributing authors: jarbas.fernandes@ufob.edu.br;
marcus.americano@ufsc.br;

Abstract

Geothermal energy, characterized by its renewable and ubiquitous nature, offers a promising avenue for sustainable power generation and large-scale energy storage. This becomes particularly noteworthy when confronting the temporal imbalances linked to the utilization of renewable energy, given the presence of heterogeneous parameters. Addressing problems in geothermal resource utilization requires a comprehensive understanding of geological attributes, aquifer and aquiclude physical characteristics, groundwater composition, and flow dynamics. Achieving precise insights into these complex processes involves the use of robust and versatile numerical simulation tools. In this context, we introduce a geothermal model for highly heterogeneous porous media, where space-dependent partially observed parameters are approximated using a conditional Karhunen-Loève expansion

(cKLE). The choice of cKLE is significant as it allows us to obtain parameters with strong variability in the spatial domain with reduced dimensionality. Within an integrated framework, we employ the Levenberg-Marquardt (LM) and Singular Value Decomposition (SVD) techniques to determine coefficients from cKLE that generate the permeability fields. These techniques are utilized in the inverse geothermal problem to iteratively identify the permeability field that minimizes misfit. A real dataset with the injection of hot water into Layer 10 of SPE 10 model under fixed-temperature boundary conditions, was used to test and validate the approach. Synthetic time data were generated for pressure and temperature. The inversion of geothermal data demonstrates that the proposed methods obtains the permeability fields with a high level of accuracy. The inversion methods based on LM and SVD combined with cKLE successfully reconstructed the heterogeneous permeability fields with high accuracy and computational efficiency, demonstrating robustness even under noisy data conditions.

Keywords: Geothermal energy, Inverse problem, Conditional Karhunen-Loéve expansion

1 Introduction

Geothermal energy is an abundant and sustainable source of renewable energy. Its utilization involves harnessing the heat stored in the Earth's underground layers, including rocks, soils, and groundwater. The integration of renewable energy sources is crucial for the decarbonization of the energy matrix, as they can contribute significantly to meeting the demand. To make these resources economically viable, a deeper understanding of energy transport in porous media is essential, reducing uncertainties in their application [1, 2].

In recent years, there has been a growing interest in accurately predicting petroleum reservoir simulations using methods that quantify uncertainties [3–6]. Geological formation variability and limited understanding of its features in heterogeneous media demand methods that can accurately reproduce parameters that vary significantly in the model. In this sense, a suitable parameterization technique is necessary to describe parameters that vary heterogeneously in porous media, while considering the minimum number of degrees of freedom in the model [7].

In this paper, a new methodology based on non-linear least squares methods is proposed to calculate the coefficients of the KLE during the parameterization of permeability fields. More specifically, this study focuses on conducting temperature analyses in wells for a compressible, single-phase problem to approximate the permeability field using cKLE. Each of these KLE is then conditioned on their corresponding measurements associated with the production wells inserted in the geometry of model. To achieve this, we will employ inversion on the permeability fields to obtain the coefficients of the KLEs by comparing findings for pressure and temperature through the misfit between the reference and approximate data. The initial model will be refined through local search regularization techniques using the Levenberg-Marquardt (LM)

algorithm [8, 9] and Singular Value Decomposition (SVD) algorithm [10, 11]. These inversion processes can provide a quick and precise evaluation of the coefficients of the KL expansion, using few sequential stages, unlike random methods that depend on a large number of samples.

A similar study involving inverse problems in partial differential equations models by representing the parameter fields using cKLEs conditioned on available direct measurements was proposed by Li and Tartakovsky [12, 13], Tartakovsky [14] and Yeung [15]. Other applications of cKLE to solving stochastic boundary value problems can be found in Chang and Zhang [16].

During the numerical discretization of governing equations, the finite volume (FV) method is employed to ensure accuracy in measuring pore pressure for fluid conservation equations and mixed formulations. Unstructured Voronoi grids are constructed using the perpendicular bisector (PEBI) grids to refine the mesh in the region of production wells [17]. Furthermore, we apply implicit discretization to ensure that the geothermal model is unconditionally related to all general polyhedral meshes. We conclude by presenting a numerical synthetic example in which we estimate the permeability field of a geothermal system using the LM and SVD approaches. The SPE 10 benchmark was widely used for testing and validating this reservoir simulation model [18].

Our motivation for this work is to estimate permeability fields in inverse problems associated with thermal field-scale flow in porous media. For this class of problems, the parameterization of these fields is typically calculated using uncertainty quantification methods such as the Markov Chain Monte Carlo Method [19, 20], Moment method [21], spectral method [22], LU matrix decomposition [23], FFT-MA method [24] and sequential simulation [25]. These methods differ in the strategy used; however, a common characteristic among them is that all depend on a significant computational effort to achieve convergence.

This paper is structured as follows. In Sections 2 and 3, we introduce the geothermal problem and its numerical formulation using finite volume method. In Section 4, we describe the procedure for parameterization of the permeability fields using cKLE. Section 5 discusses the inversion procedures, while in Section 6, the LM and SVD schemes are presented along with their respective algorithms. In Section 7, we apply the proposed methodology to an inversion problem from Layer 10 in the SPE 10 benchmark (including free and noisy examples investigating the stability of the method with purely and contaminated data) with a five-spot geometry. Conclusions and discussions are presented in Section 8 and 9, respectively.

2 Geothermal Model

We begin by introducing the geothermal model utilized in our simulations, which is employed to discretize the fundamental equations governing single-phase, compressible flow through the application of discrete differential and averaging operators. The governing single-phase equations for thermal field-scale flow in porous media typically consist of the following equations:

Darcy's Law: This equation describes a fluid flow in porous media based on pressure gradients:

$$\mathbf{u} = -\frac{\mathbf{K}}{\mu}(\nabla p - \rho \mathbf{g} \nabla z) \tag{1}$$

where:

- $\mathbf{u}$: Darcy velocity (velocity of the fluid phase) [m/s]
- $\mathbf{K}$: Permeability tensor [m^2]
- μ: Dynamic viscosity of the fluid [cP·s]
- p: Pressure [Pa (Pascal)]
- ρ: Fluid density [kg/m^3]
- $\mathbf{g}$: Gravitational acceleration vector [m/s^2]

We will assume that $\mathbf{K}$ is isotropic tensor defined by $\mathbf{K} = \kappa(\mathbf{x})\mathbf{I}$, where $\mathbf{I}$ is a unit matrix and $\kappa(\mathbf{x})$ is a scalar function. The permeability κ will be considered a random parameter.

Conservation of Mass: The equation states that the rate of change of an arbitrary fluid mass within a control volume is equal to the net fluid inflow/outflow rate defined by:

$$\rho S \frac{\partial p}{\partial t} + \nabla \cdot (\rho \mathbf{u}) = Q_M \tag{2}$$

where Q_M [W/m^3] is the source/sink term and S [m^3] is rock storage coefficient.

Conservation of Energy (Heat Transport Equation): This equation describes the temperature distribution and heat transfer within the porous media

$$\frac{\partial}{\partial t}[\phi \rho E_f(p,t) + (1-\phi)E_r] + \nabla \cdot (\rho H_f \mathbf{u}) - \nabla \cdot (\kappa_T \nabla T) = Q_T \tag{3}$$

where:

- E_f: Energy density per mass of the fluid [J/kg]
- E_r: Energy per volume of the rock [J/m^3]
- $H_f = E_f + p/\rho$: Enthalpy density per mass [J/kg]
- T: Temperature [K (Kelvin)]
- c: Specific heat capacity [J/(kg·K)]
- κ_T: Thermal conductivity [W/(m·K)]
- Q_T: Heat source/sink term [W/m^3]
- ϕ: Porosity

Since we are working with a compressible fluid medium, the fluid density (ρ) and viscosity (μ) can be mathematically related to pressure, temperature through the following equations of state:

$$\begin{aligned} \rho(p,T) &= \rho_r[1 + \beta_T(p - p_r)]e^{-\alpha(T-T_r)}, \\ \mu(p,T) &= \mu_0[1 + c_\mu(p - p_r)]e^{-c_T(T-T_r)}, \end{aligned} \tag{4}$$

such that, $\rho_r = 850\,\mathrm{kg/m^3}$ represents the density, and $\mu_0 = 5\,\mathrm{cP}$ stands for the viscosity of the water under reference conditions, characterized by a pressure $p_r = 200 \times 10^5\,\mathrm{Pa}$ and a temperature $T_r = 300\,\mathrm{K}$. The constants are defined as follows: $\beta_T = 10^{-8}\,\mathrm{Pa^{-1}}$, $\alpha = 5 \times 10^{-3}\,\mathrm{K^{-1}}$, $c_\mu = 2 \times 10^{-8}\,\mathrm{Pa^{-1}}$, and $c_T = 10^{-3}\,\mathrm{K^{-1}}$.

In order to calculate the enthalpy, we use a simple linear relationship based on thermodynamic relationships:

$$dH_f = c_p dT + \left(\frac{1-\alpha T_r}{\rho}\right) dp, \quad \alpha = -\frac{1}{\rho}\frac{\partial \rho}{\partial T}|_p \tag{5}$$

where $c_p = 4 \times 10^3 \ J/kg$.

3 Numerical approximation

In this section, a finite volume formulation is used to derive approximate solutions for Eqs. (1)-(3).

3.1 Discrete Operators and Equations

Following Krogstad et al. [26], we will use the same notation to construct this discrete problem. Let n_c be the number of cells and n_f the corresponding number of faces. Consider the mapping $F : \{1, \ldots, n_c\} \to \{0, 1\}^{n_f}$ from the cell to a set of faces and mappings $N_1, N_2 : \{1, \ldots, n_f\} \to \{1, \ldots, n_c\}$ from the face to the two neighboring cells. We also define the discrete versions of the gradient and divergent operators as **grad** and **div**, respectively.

Let us denote by $\mathbf{u} \in \mathbb{R}^{n_f}$ the discrete flux while $\mathbf{u}|_f$ represents its restriction onto face f with orientation from $N_1(f)$ to $N_2(f)$. In this case, the discrete divergence operator **div** evaluated in the flow $\mathbf{v}$ and restricted to cell $\mathcal{C}$ is written as:

$$\mathbf{div}(\mathbf{u})|_{\mathcal{C}} = \sum_{f \in F(\mathcal{C})} \mathbf{u}|_f \chi(\mathcal{C} = N_1(f)) - \sum_{f \in F(\mathcal{C})} \mathbf{u}|_f \chi(\mathcal{C} = N_2(f)). \tag{6}$$

Similarly, the discrete gradient **grad** on the face f is expressed by:

$$\mathbf{grad}(\mathbf{p})|_f = \mathbf{p}|_{N_2(f)} - \mathbf{p}|_{N_1(f)}, \tag{7}$$

for any $\mathbf{p} \in \mathbb{R}^{n_c}$. The discrete flux is defined by

$$\mathbf{u} = -\mathbf{upw}(1/\mu)|_f \mathbf{K} \left(\mathrm{grad}(\mathbf{p}) - g \ avg(\mathbf{p})\mathbf{grad}(\mathbf{z})\right)|_f, \tag{8}$$

Here, the operator **upw** represents the phase-upwind function:

$$\mathbf{upw}(\tau)|_f = \begin{cases} \tau|_{N_1(f)} & \text{if } \mathbf{grad}(\mathbf{p})|_f - g \ \mathrm{avg}(\mathbf{p})\mathbf{grad}(\mathbf{z})|_f > 0 \\ \tau|_{N_2(f)} & \text{otherwise.} \end{cases}$$

while $avg(\mathbf{p})$ denotes the arithmetic average of the face-valued pressure in the two adjacent cells, i.e:

$$avg(\mathbf{p}) = \frac{1}{2}(\mathbf{p}|_{N_1(f)} + \mathbf{p}|_{N_2(f)}) \tag{9}$$

3.2 Discretization of the flow equations using FV

To calculate the time derivative of Eq. (2), it is necessary to perform a time integration. Therefore, it is advantageous to partition the time interval $I = [0, T]$ into sub-intervals of size Δt, i.e, $0 = t^0 \leq t^1 \leq \ldots \leq t^{N_t} = T$ such that $t^n = t^{n-1} + \Delta t$. Integrating Eq. (2) over a specific time interval from t to $t + \Delta t$ and spatial domain Ω, we obtain:

$$\int_t^{t+\Delta t} \int_\Omega \rho S \frac{\partial p}{\partial t} + \nabla \cdot (\rho \mathbf{u})\, d\Omega dt = \int_t^{t+\Delta t} \int_\Omega Q_M \, d\Omega dt \tag{10}$$

$$\begin{aligned} &\textstyle\int_t^{t+\Delta t} \int_\Omega \frac{\partial}{\partial t}[\phi \rho E_f(p,t) + (1-\phi)E_r] + \nabla \cdot (\rho H_f \mathbf{u})\, d\Omega dt \\ &\textstyle - \int_t^{t+\Delta t} \int_\Omega \nabla \cdot (\kappa_T \nabla T)\, d\Omega dt = \int_t^{t+\Delta t} \int_\Omega Q_T \, d\Omega dt. \end{aligned} \tag{11}$$

In our approach, we aim to approximate the solution p at time t^n for each $n = 1, \ldots, N_t$, where N_t represents the number of measurements in time based on the uniform discretization of the interval $[0, T]$. Using an implicit first-order backward-Euler scheme in time, we have:

$$S\left(\frac{(\boldsymbol{\rho}\mathbf{p})^{n+1} - (\boldsymbol{\rho}\mathbf{p})^n}{\Delta t}\right)|_{\mathcal{C}} + \mathbf{div}((avg(\boldsymbol{\rho})\mathbf{u})^{n+1}|_{\mathcal{C}} = (\mathbf{Q_M})^{n+1}|_{\mathcal{C}} \tag{12}$$

$$\begin{aligned} &\textstyle\frac{(\boldsymbol{\phi}\boldsymbol{\rho}E_f(\mathbf{p}))^{n+1} - (\boldsymbol{\phi}\boldsymbol{\rho}E_f(\mathbf{p}))^n}{\Delta t}|_{\mathcal{C}} + \frac{((1-\boldsymbol{\phi})E_r)^{n+1} - ((1-\boldsymbol{\phi})E_r)^n}{\Delta t}|_{\mathcal{C}} \\ &+\mathbf{div}((\mathbf{upw}(H_f)avg(\boldsymbol{\rho})\mathbf{u})^{n+1}|_{\mathcal{C}} - \mathrm{div}(\mathbf{upw}(\kappa_T)\mathbf{u})^{n+1}|_{\mathcal{C}} = (\mathbf{Q_T})^{n+1}|_{\mathcal{C}}. \end{aligned} \tag{13}$$

The variables $\boldsymbol{\phi}$, $\boldsymbol{\rho}$, $\mathbf{p} \in \mathbb{R}^{n_c}$ denote vectors with one porosity value, one density, and one pressure value per cell, respectively, whereas $\mathbf{u}$ is the vector of fluxes per face, and so on.

3.3 Well production

The production well is incorporated as a source term in the pressure equation, necessitating the definition of a flow rate expression for all cells connected to the reservoir via the well (referred to as well connections). Within the well itself, we assume instantaneous flow, ensuring that the pressure drop remains hydrostatic at all times. Assuming a constant fluid density within the well, computed at the bottom-hole pressure $\mathbf{p}_{bh}$, the pressure $\mathbf{p}_c[w]$ in connection grid cell w of well $N_w(w)$ is given by:

$$\mathbf{p}_c|_w = \mathbf{p}_{bh}|_{N_w(w)} + g\boldsymbol{\Delta}\mathbf{z}\rho(\mathbf{p}_{bh}|_{N_w(w)}) \tag{14}$$

Thus the mass flow-rate is defined by:

$$\mathbf{q}_c|_w = \frac{\rho(\mathbf{p}|_{N_c(w)})}{\mu} W_i|_w(\mathbf{p}_c|_w - \mathbf{p}|_{N_c(w)}) \tag{15}$$

where $\mathbf{p}|_{N_c(w)}$ is the pressure in cell $N_c(w)$ containing connection w and W_i is the well of index i (see [18, page 208]).

4 Parameterization by Karhunen-Loève expansion

To construct Gaussian random fields related to permeability through the inversion method, we typically employ the traditional Karhunen-Loève expansion (KLE) [3, 27, 28] of a random field Y:

$$Y(\boldsymbol{x};\omega) = \bar{Y}(\boldsymbol{x}) + \sum_{k=1}^{\infty} \sqrt{\lambda_k} f_k(\boldsymbol{x}) \xi_k(\omega), \tag{16}$$

where, $\xi_k(\omega)$, $k = 1, 2, \ldots$, represents independent random variables to be determined and $\bar{Y}(\mathbf{x}) = \mathbb{E}[Y(\boldsymbol{x};\omega)]$. Here the expressions λ_k and $f_k(\boldsymbol{x})$ are respectively the eigenvalues and eigenfunctions utilized in the parameterization of the permeability field by KLE and obtained from Fredholm integral equation of second kind:

$$\int_{\mathcal{R}} C_Y(\boldsymbol{x},\boldsymbol{y}) f_k(\boldsymbol{y})\, d\boldsymbol{y} = \lambda_k f_k(\boldsymbol{x}), \quad k = 1, 2, \ldots. \tag{17}$$

Due to the infinite nature of the sum in Eq. (21), the KLE in this form cannot be directly used for numerical calculations. Therefore, for computational purposes, we will limit the KLE to a finite number M of terms. In this case, we could rewrite the truncated expression of Eq. (21) as

$$Y(\boldsymbol{x};\omega) = \bar{Y}(\boldsymbol{x}) + \sum_{k=1}^{M} \sqrt{\lambda_k} f_k(\boldsymbol{x}) \xi_k(\omega), \tag{18}$$

where $\{f_k\}_{k=1}^{M}$ is orthonormal set of the deterministic eigenfunctions on $L_2(\mathcal{R})$. In this situation, the eigenvalues and eigenfunctions can be determined by a numerical approximation of the eigenvalue problem Eq. (17). We carry out this approximation by the piecewise-constant finite element method (see [29] for details).

In this work, we will consider the ξ_k's with $k = 1, \ldots, M$ not as random variables but as coefficients of KLE. Thus, we aim to represent the permeability fields as a function that fits the observed data in terms of these coefficients (see [14] for details). In this context, we will treat the KLE as a deterministic representation of measurements of Y, where the coefficients of the field will be conditioned on the observed data. Assuming that measurements of Y are known in the domain $\mathcal{R}$ at locations $\boldsymbol{x}_j$, with Gaussian noise $\eta_j \sim N(0, \sigma_\eta^2)$ for $j = 1, \ldots, N_g$, where N_g is the number of mesh points, we can define the mean and the covariance matrix of the conditioned field Y respectively as follows:

$$\bar{Y}^c(\boldsymbol{x}) = \bar{Y}(\boldsymbol{x}) + R(\boldsymbol{x}) \left[\Sigma + \sigma_\eta^2 I\right]^{-1} K, \tag{19}$$

$$C_Y^c(\boldsymbol{x},\boldsymbol{y}) = C_Y(\boldsymbol{x},\boldsymbol{y}) - R(\boldsymbol{x}) \left[\Sigma + \sigma_\eta^2 I\right]^{-1} R(\boldsymbol{y}). \tag{20}$$

where

$$R(\boldsymbol{z}) = [C_Y(\boldsymbol{z}, \boldsymbol{y}_1), CY(\boldsymbol{z}, \boldsymbol{y}_2), \ldots, CY(\boldsymbol{z}, \boldsymbol{y}_{N_g})], \quad \text{for any } \boldsymbol{z} \in \mathcal{R},$$
$$\Sigma = [C_Y(\boldsymbol{x}_i, \boldsymbol{y}_j)], \quad \text{for } i, j = 1, \ldots, N_g,$$
$$K = [Y_1 - \bar{Y}(\boldsymbol{x}_1), Y_2 - \bar{Y}(\boldsymbol{x}_2), \ldots, Y_{N_g} - \bar{Y}(\boldsymbol{x}_{N_g})].$$

Thus, we can write the truncated expression for the conditional Karhunen-Loève expansion (cKLE) by:

$$Y^c(\boldsymbol{x}, \boldsymbol{\xi}) = \bar{Y}^c(\boldsymbol{x}) + \sum_{k=1}^{M} \sqrt{\lambda_k^c} f_k^c(\boldsymbol{x}) \xi_k, \tag{21}$$

where $\boldsymbol{\xi} = [\xi_1, \ldots, \xi_M]^T$ is a vector of unknown parameters (as opposed to a vector of random variables in the forward uncertainty quantification problem), and $\{\lambda_i^c, f_i^c\}_{i=1}^M$ are the first M pairs of eigenvalues and eigenfunctions stemming from the eigenvalue problem

$$\int_{\mathcal{R}} C_Y^c(\boldsymbol{x}, \boldsymbol{y}) f^c(\boldsymbol{y}) \, \mathrm{d}\boldsymbol{y} = \lambda^c f^c(\boldsymbol{x}),$$

where C_Y^c is given by (20). In this context, $\{f_k^c\}_{k=1}^M$ is orthonormal set of the deterministic functions on $L_2(\mathcal{R})$.

In the applications, we consider the Gauss covariance function

$$C_Y(\boldsymbol{x}, \boldsymbol{y}) = \sigma_Y^2 \exp\left(-\frac{\|\boldsymbol{x} - \boldsymbol{y}\|_2^2}{2\ell^2}\right). \tag{22}$$

where ℓ is the correlation length and $\sigma_Y^2 = E(Y^2)$ is the variance.

In this experiment we set the prior in permeability field κ:

$$\kappa(\boldsymbol{x}, \boldsymbol{\xi}) = 2 \times 10^{-14} \cdot \exp(Y_M^c(\boldsymbol{x}, \boldsymbol{\xi})), \tag{23}$$

which can be reformulated in terms of the vector $\boldsymbol{\xi}$ associated with the cKLE (18), as follows:

$$\kappa(\boldsymbol{x}, \boldsymbol{\xi}) = \kappa(\boldsymbol{\xi}) = \kappa(\xi_1, \ldots, \xi_M). \tag{24}$$

Hence, the estimation of the permeability field $\kappa(\boldsymbol{\xi})$ is simplified by estimating the M-dimensional parameter vector $\boldsymbol{\xi}$.

4.1 Criterion-based space dimensionality reduction

According to [14], follows that the bulk variance is given by:

$$\int_{\mathcal{R}} Var(Y^c(\boldsymbol{x})) d\boldsymbol{x} = \sum_{k=1}^{\infty} \lambda_k^c. \tag{25}$$

This equation can be used to reduce the spatial dimensionality associated with the parameterization of fields. Let us construct a reduced-dimensionality space provided that

$$\sum_{k=1}^{M} \lambda_k \geq l \sum_{k=1}^{\infty} \lambda_k, \tag{26}$$

where l, $0 < l \leq 1$, is the desired level of confidence for the shape modification variability as defined in Eq. (25), with $\lambda_k \geq \lambda_{k+1}$. This dimension reduction criterion given by Eq. (26) will assist in the optimization of the inversion process by minimizing the objective function. Furthermore, we can accurately estimate the various fields that can be evaluated during the parameterization process.

5 Inversion Procedure

The inverse problem involves determining a model that minimizes the misfit between observed and estimated data. In this situation, let us designate vectors $\mathbf{d}^{\text{ref}}$ and $\mathbf{d}$ as the observed and estimated data by

$$\begin{aligned} \mathbf{d}^{\text{ref}} &= [\mathbf{d}_1^{\text{ref}}, \ldots, \mathbf{d}_{N_w}^{\text{ref}}]^T \\ \mathbf{d}(\boldsymbol{\xi}) &= [\mathbf{d}_1^{\text{est}}(\boldsymbol{\xi}), \ldots, \mathbf{d}_{N_w}^{\text{est}}(\boldsymbol{\xi})]^T \end{aligned} \tag{27}$$

respectively, where the parameter $\boldsymbol{\xi}$ represents the sought-after coefficient of cKLE associated with the permeability field $\kappa(\boldsymbol{\xi})$.

Note that the vectors $\mathbf{d}_i^{\text{ref}}$ and $\mathbf{d}_i$ represent the reference and estimated values, respectively, in the production wells over a specified time period. Thus, we can define these vectors as follows:

$$\begin{aligned} \mathbf{d}_i^{\text{ref}} &= [p_{1i}, \ldots, p_{N_t i}, T_{1i}, \ldots, T_{N_t i}]^T, \quad i = 1, \ldots, N_w \\ \mathbf{d}_i^{\text{est}}(\boldsymbol{\xi}) &= [p_{1i}(\boldsymbol{\xi}), \ldots, p_{N_t i}(\boldsymbol{\xi}), T_{1i}(\boldsymbol{\xi}), \ldots, T_{N_t i}(\boldsymbol{\xi})]^T. \end{aligned} \tag{28}$$

in that N_t denotes the number of time measurements, and N_w is the count of production wells associated with pressure p_{ji} and temperature T_{ji} solutions, where $j = 1, \ldots, N_t$, $i = 1, \ldots, N_w$. Due to this, we will have a total of $N_d = N_t \cdot N_w$ data, so that we can rewrite the vectors defined in Eq. (27) as follows:

$$\begin{aligned} \mathbf{d}^{\text{ref}} &= [d_1^{\text{ref}}, \ldots, d_{N_d}^{\text{ref}}]^T \\ \mathbf{d}(\boldsymbol{\xi}) &= [d_1, \ldots, d_{N_d}]^T. \end{aligned} \tag{29}$$

In order to quantify the misfit between the observed and estimated data, we will address the following nonlinear least-squares problem: Find the coefficient vector $\boldsymbol{\xi}$ that minimizes the objective function:

$$\min_{\boldsymbol{\xi} \in \mathbb{R}^M} \Phi(\boldsymbol{\xi}), \quad \Phi(\boldsymbol{\xi}) = \frac{\sum_{i=1}^{N_d} (d_i^{ref} - d_i(\boldsymbol{\xi}))^2}{\sum_{i=1}^{N_d} (d_i^{ref})^2}, \tag{30}$$

The values that minimize the misfit expression in Eq. (30) are computed using the LM and SVD algorithms summarized in the next section.

6 Inverse methodology

We recall the classical LM and SVD algorithms for inferring the vector $\boldsymbol{\xi}$ associated with the permeability field $\kappa(\boldsymbol{\xi})$. In both algorithms, the initial vector $\boldsymbol{\xi}^{(0)}$ is selected from a standard Gaussian distribution $N(\mathbf{0}, \mathbf{I})$.

6.1 Levenberg-Marquadt (LM) algorithm

The initial vector $\boldsymbol{\xi}^{(0)}$ can be refined by solving the following nonlinear least-squares problem

$$g(\boldsymbol{\xi}) = \min_{\boldsymbol{\xi} \in \mathbb{R}^M} \frac{1}{2} \|\mathbf{d}(\boldsymbol{\xi})\|_2^2. \tag{31}$$

To determine the numerical solution to this problem, we employ the classical Levenberg-Marquardt method:

$$\left((\mathbf{J}^{(k)})^T \mathbf{J}^{(k)} + \mu_k \mathbf{I} \right) \mathbf{p}^{(k)} = (\mathbf{J}^{(k)})^T \mathbf{d}^{(k)} \tag{32}$$

$$\boldsymbol{\xi}^{(k+1)} = \boldsymbol{\xi}^{(k)} + \alpha_k \mathbf{p}^{(k)}, \tag{33}$$

where $\mathbf{d}^{(k)} = \mathbf{d}(\boldsymbol{\xi}^{(k)})$. Here, $\mu_k > 0$ is referred to as the damping parameter, ensuring the invertibility of the matrix $\left((\mathbf{J}^{(k)})^T \mathbf{J}^{(k)} + \mu_k \mathbf{I} \right)$, and $\alpha_k > 0$ represents the step size. The criteria for calculating the parameters μ_k and α_k are motivated by the work of Yamashita and Fukushima [9], whose the choice of the damping parameter is given by $\mu_k = \mu(\boldsymbol{\xi}^{(k)}) := \|\mathbf{d}(\boldsymbol{\xi}^{(k)})\|_2^2$, for all $k \geq 0$. On the other hand, the step α_k is determined by the Armijo's Criterion. In this case, given scalars $0 < \nu, \eta < 1$, the step is chosen as the smallest non-negative integer m that satisfies:

$$g(\boldsymbol{\xi}^{(k)} + \eta^m \mathbf{p}^{(k)}) - g(\boldsymbol{\xi}^{(k)}) \leq \nu \eta^m \nabla g(\boldsymbol{\xi}^{(k)})^T \mathbf{p}^{(k)},$$

so that $\alpha_k = \eta^m$.

In this process, the update vector $\mathbf{p}^{(k)}$ is determined by solving a least-squares system involving the $N_d \times M$ sensitivity matrix $\mathbf{J}^{(k)}$. The entries of $\mathbf{J}^{(k)}$ are given as follows:

$$J_{ij}^{(k)} = \frac{\partial d_i}{\partial \xi_j}(\boldsymbol{\xi}^{(k)}) \quad (1 \leq i \leq N_d, \quad 1 \leq j \leq M). \tag{34}$$

A summary of the proposed is given in **Algorithm 1**.

Algorithm 1: LM algorithm

Input: $tol, \nu, \eta \in (0,1)$, $\mathbf{d}, \mathbf{J}, \mathbf{I}$, and $\boldsymbol{\xi}^{(0)} \in \mathbb{R}^M$;
$\mu_0 = \|\mathbf{d}(\boldsymbol{\xi}^{(0)})\|_2^2$
for $k = 0, 1, \ldots$ **do**
  if $\Phi(\boldsymbol{\xi}^{(k)}) \leq tol$ **then**
    Stopping criterion is satisfied.
  else
    Find the solution $\mathbf{p}^{(k)}$: $\mathbf{p}^{(k)} = -((\mathbf{J}^{(k)})^T\mathbf{J}^{(k)} + \mu_k(\mathbf{I}))^{-1}(\mathbf{J}^{(k)})^T\mathbf{d}^{(k)}$
  end
  if $\|\mathbf{d}(\boldsymbol{\xi}^{(k)} + \mathbf{p}^{(k)})\|_2^2 < \|\mathbf{d}(\boldsymbol{\xi}^{(k)})\|_2^2$ **then**
    $\alpha_k = 1$
  else
    Choose m as the smallest non-negative integer such that:
    $g(\boldsymbol{\xi}^{(k)} + \eta^m\mathbf{p}^{(k)}) - g(\boldsymbol{\xi}^{(k)}) \leq \nu\eta^m\nabla g(\boldsymbol{\xi}^{(k)})^T\mathbf{p}^{(k)}$;
    $\alpha_k = \eta^m$
  end
  $\boldsymbol{\xi}^{(k+1)} = \boldsymbol{\xi}^{(k)} + \alpha_k\mathbf{p}^{(k)}$
  $\mu_{k+1} = \|\mathbf{d}(\boldsymbol{\xi}^{(k+1)})\|_2^2$
end

6.2 Singular value decomposition (SVD) algorithm

Following [10, 11] we have formulated an iterative equation for updating vector parameters using the idea of factorizing the Jacobian matrix $\mathbf{J}^{(k)}$, $k = 0, 1, \ldots$ defined in Eq. (34) into three other matrices as follows:

$$\mathbf{J}(\boldsymbol{\xi}^{(k)}) = \mathbf{J}^{(k)} = \mathbf{U}\mathbf{S}\mathbf{V}^T, \quad k = 0, 1, \ldots \tag{35}$$

where $\mathbf{U}$ is $(N_d \times M)$ data left singular vectors, $\mathbf{V}$ is $(M \times M)$ model parameters right singular vectors, and $\mathbf{S}$ is $(M \times M)$ matrix with η_i, $i = 1, \ldots, M$ singular values of $\mathbf{J}^{(k)}$ in its diagonal. In the least squares problem, the matrix $(\mathbf{J}^{(k)})^T\mathbf{J}^{(k)}$ is usually ill-conditioned in case of small singular values. This can lead to divergence in the inversion matrix, so a small perturbation term is added to the eigenvalues of $(\mathbf{J}^{(k)})^T\mathbf{J}^{(k)}$. Thus, the least square problem can be expressed as follows:

$$((\mathbf{J}^{(k)})^T\mathbf{J}^{(k)} + \lambda I)\Delta\boldsymbol{\xi} = -(\mathbf{J}^{(k)})^T\Delta\mathbf{d}, \tag{36}$$

where $\Delta\boldsymbol{\xi} = \boldsymbol{\xi}^{(k+1)} - \boldsymbol{\xi}^{(k)}$, and $\Delta\mathbf{d} = \mathbf{d}^{\text{ref}} - \mathbf{d}(\boldsymbol{\xi}^{(k)})$. Here, Eq. (36) can be rewritten in terms of the decomposition matrices $\mathbf{U}$, $\mathbf{S}$ and $\mathbf{V}$ as follow

$$(\mathbf{V}\mathbf{S}^{\mathbf{2}}\mathbf{V}^T + \lambda\mathbf{I})\Delta\boldsymbol{\xi} = -(\mathbf{V}\mathbf{S}\mathbf{U}^T)\Delta\mathbf{d}, \tag{37}$$

The left-hand side of Eq. (37) can be rewritten as:

$$(\mathbf{V}\mathbf{S}^{\mathbf{2}}\mathbf{V}^T + \lambda\mathbf{I}) = (\mathbf{V}\text{diag}(\eta_i^2)\mathbf{V}^T) + \lambda^2\mathbf{I} = \mathbf{V}\text{diag}(\eta_i^2 + \lambda^2)\mathbf{V}^T, \tag{38}$$

where η_i is the i-th eigenvalue. The following equation shows the inverse of Eq. (38):

$$(\mathbf{V}\text{diag}(\eta_i^2 + \lambda^2)\mathbf{V}^T)^{-1} = \mathbf{V}\text{diag}\left(\frac{\eta_i}{\eta_i^2 + \lambda^2}\right)\mathbf{V}^T. \tag{39}$$

Consequently, the solution vector obtained based on SVD is given by:

$$\boldsymbol{\xi}^{(k+1)} = \boldsymbol{\xi}^{(k)} + \mathbf{V}\text{diag}\left(\frac{\eta_i}{\eta_i^2 + \lambda_k^2}\right)\mathbf{U}^T\Delta\mathbf{d}. \tag{40}$$

The damping factor λ has been updated in terms of the misfit $\Phi(\boldsymbol{\xi}^{(k)})$ through the following equation:

$$\lambda_k = \eta_k(\Delta\Phi(\boldsymbol{\xi}^{(k)}))^{1/k}, \tag{41}$$

in that $\Delta\Phi(\boldsymbol{\xi}^{(k)})$ can be given by:

$$\Delta\Phi(\boldsymbol{\xi}^{(k)}) = \frac{\Phi(\boldsymbol{\xi}^{(k)}) - \Phi(\boldsymbol{\xi}^{(k-1)})}{\Phi(\boldsymbol{\xi}^{(k-1)})}, \tag{42}$$

where $\Phi(\boldsymbol{\xi}^{(k-1)})$ and $\Phi(\boldsymbol{\xi}^{(k)})$ are the misfits of the previous and present iterations, respectively. A summary of this algorithm is given below:

Algorithm 2: SVD algorithm

Input: $tol, \mathbf{J}^{(0)}$, and $\boldsymbol{\xi}^{(0)} \in \mathbb{R}^M$;
Perform SVD on $\mathbf{J}^{(0)}$: $\mathbf{J}^{(0)} = \mathbf{U}\mathbf{S}\mathbf{V}^T$
for $k = 0, 1, \ldots$ **do**
  if $\Phi(\boldsymbol{\xi}^{(k)}) \leq tol$ **then**
    Stopping criterion is satisfied.
  else
    Find the solution $\boldsymbol{\xi}^{(k)}$: $\boldsymbol{\xi}^{(k+1)} = \boldsymbol{\xi}^{(k)} + \mathbf{V}\text{diag}\left(\frac{\eta_i}{\eta_i^2+\lambda_k^2}\right)\mathbf{U}^T\Delta\mathbf{d}$.
  end
  if $\Phi(\boldsymbol{\xi}^{(k+1)}) < \Phi(\boldsymbol{\xi}^{(k)})$ **then**
    $\lambda_{k+1} = \eta_k(\Delta\Phi(\boldsymbol{\xi}^{(k)}))^{1/k}$
    $\Delta\Phi(\boldsymbol{\xi}^{(k)}) = \frac{\Phi(\boldsymbol{\xi}^{(k)})-\Phi(\boldsymbol{\xi}^{(k-1)})}{\Phi(\boldsymbol{\xi}^{(k-1)})}$,
  else
    $\lambda_{k+1} = \lambda_k$
  end
  Perform SVD on $\mathbf{J}^{(k)}$: $\mathbf{J}^{(k)} = \mathbf{U}\mathbf{S}\mathbf{V}^T$
end

7 Numerical test

This numerical test use the SPE 10 model 2 described in [17], which apply a perpendicular bisector (PEBI) grid with refinement around the production well. We use the *upr* module described in [18] to create a PEBI grid. It utilized a sedimentary bed model with six rock types, featuring a corner-point grid setup with $13,200$ cells. At the fine geological model scale, the model is described on a regular Cartesian grid with dimensions of 60×220.

We examine an inverted five-spot pattern. In contrast to the producers, which are run at a constant bottom-hole pressure (BHP) of 275.8×10^5 Pa, the center well continuously injects $373.15^o K$ water at a rate of 50 m^3 per day. We impose no-flow boundary conditions on all sides and take a thermally insulated boundary condition, indicating that no heat exchange occurs between the system and its surroundings across those borders. An illustration of the boundary and initial conditions can be found in Figure 1 on PEBI grid.

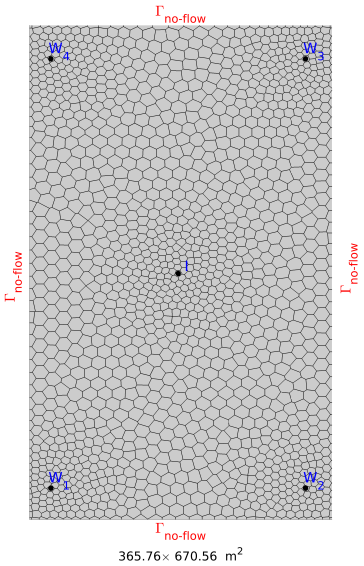


Fig. 1: Initial and boundary conditions for the five-spot scheme in the case study. The symbols "•" denote the locations where the pressure and temperature sensors are known, and the symbol W_i, $i = 1, \ldots 4$ indicate the production wells and I indicate the injection well.

In order to construct this inverse model, we first used noise-free data from the four production wells in a simulation period of $[0, T] = [0, 2000]$ days divided into $\Delta t = 30$ days equally-spaced time steps, to simulate injection of hot water into SPE 10 model. The reservoir parameters, production data, and other extra parameters are given in Table 1.

Table 1: Parameters for the Oil - Water Model

Initial pressure	$P_0 = 413.7 \times 10^5\ Pa$
Minimum temperature	$T_{min} = 273.15^o K$
Maximum temperature	$T_{max} = 548.15^o K$
Oil viscosity	$\mu_o = 3\ cP$
Rock compressibility	$c_R = 1.4494 \times 10^{-10}/Pa$
Water density	$\rho_w = 64\ lb/ft^3$
Oil density	$\rho_o = 53\ lb/ft^3$

The porosity field in a heterogeneous porous medium was fixed, while the reference solution was computed using a random sample from the permeability field. Next, we consider the Gauss covariance function with parameters $\sigma_Y = 1$ and $\ell = 100$. Using Eq. (26), we found that more than 95% of the variance in the cKLE is captured by the first 20 dominant eigenvalues. Consequently, $M = 20$ is sufficient for the size of the stochastic dimension.

Next, we calculated the misfit in Eq. (30) of the LM and SVD algorithms in the noise-free experiment. In the LM algorithm, the misfit was reduced from 0.59291 to 0.01147 over 100 iterations, while in the SVD algorithm, it decreased from 0.38788 to 0.03147 over 30 iterations. The results show that the calculated data using the LM has a better fitting than the calculated data from the SVD method.

Figures 2 to 3, reference data (solid lines) are compared with the best-fitted permeability field obtained from both LM and SVD simulations (dashed lines) for pressure and temperature in wells W_i, $i = 1, \ldots, 4$. These simulations were conducted using the initially selected vector $\boldsymbol{\xi}$ from the Gaussian samples, followed by refinement via the SVD and LM algorithms over a time span ranging from 0 to 2000 days. The dashed line represents the initial model obtained from $\boldsymbol{\xi}^{(0)}$ as well as the best-fitted model derived from the misfit equation (30). It is worth noting that the pressure and temperature solutions attained in all wells via the SVD and LM algorithms are significantly closer to the target solution.

Figure 4 displays the log-permeability fields of the initial state and reference, as well as those numerically approximated by the LM and SVD algorithms, accompanied by their respective relative errors. Notably, a significant enhancement in the permeability field is observed upon applying the LM and SVD algorithms as illustrated in Figure 4c. The comparison of relative errors between the LM and the combined SVD demonstrates the superiority of LM in our new methodology (see Figures 4f- 4e). Although the LM algorithm achieved a smaller error in the fields, it required a greater number of iterations, while the SVD algorithm obtained similar results with fewer iterations.

To evaluate the stability of the proposed LM and SVD algorithms, we introduced random Gaussian noise (RGN) at a noise percentage of 2%. In both algorithms, 100 iterations were required. When applying the algorithms to the noisy data, the optimal permeability field of the retrieved geothermal model corresponds to the minimum of the objective function (29). In this case, the misfit of the SVD algorithm decreased from 0.36488 to 0.23809, while in the LM algorithm, the misfit decreased from 0.61863 to 0.37393. Figures 5 - 6 depict the production data, including pressure and temperature

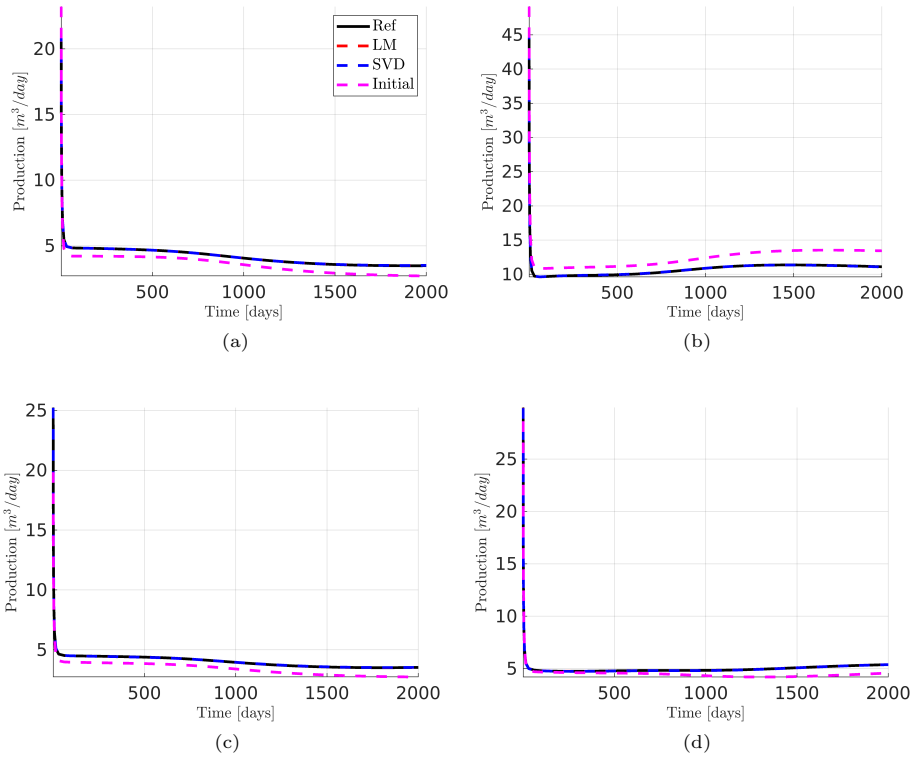


Fig. 2: Numerical Model: noise-free numerical example of the production rate SP10 model. Production rates of the water production rate versus time, associated with production wells W_1 (a), W_2 (b), W_3 (c) and W_4 (d). Solid lines denote the reference solution and dashed line the initial, optimal approximation from LM and SVD.

respectively, contaminated with 2% noise. We can observe that the LM algorithm did not provide a good approximation in well W_1. However, in the other wells, both methods showed good accuracy despite the noise. Figure 7 plots the permeability fields recovered by inversion with noise in the observation data. Both algorithms achieved similar results in the permeability fields; however, the inverse fields obtained did not match the target permeability field.

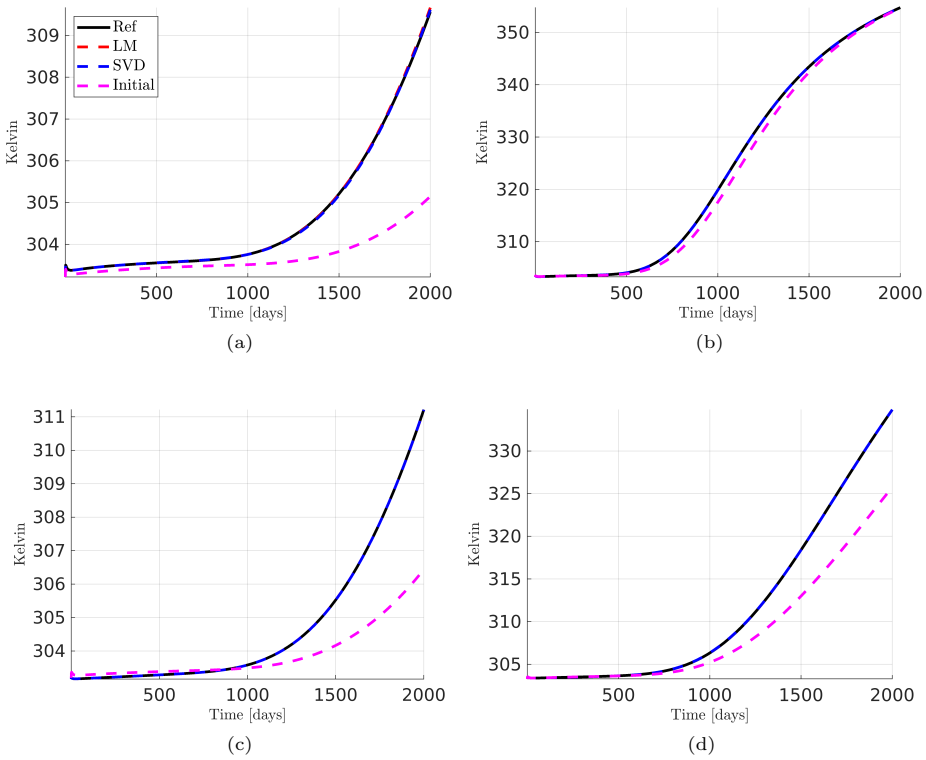
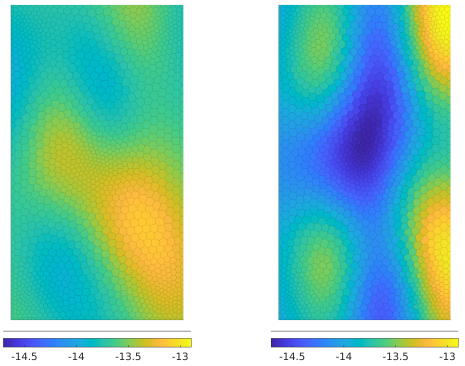
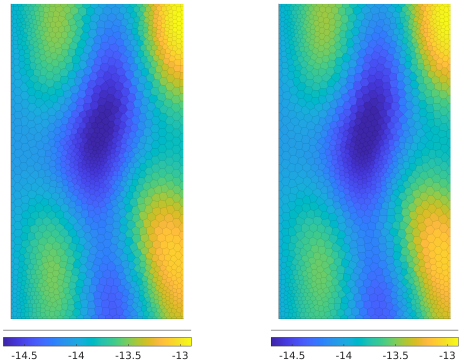


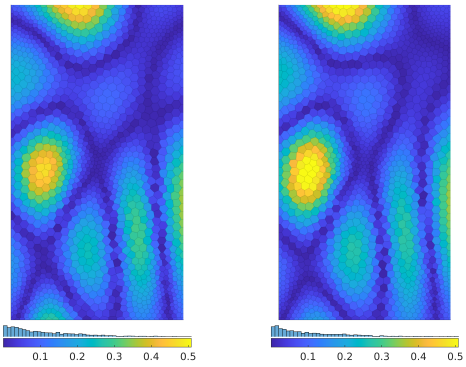
Fig. 3: Numerical Model: noise-free numerical example of the temperature SP10 model. Temperature versus time, associated with production wells W_1 (a), W_2 (b), W_3 (c) and W_4 (d). Solid lines denote the reference solution and dashed line the initial, optimal approximation from LM and SVD.



(a) Initial (b) Ref



(c) LM (d) SVD



(e) LM (f) SVD

Fig. 4: True, Initial and Recovered fields of the noisy-free numerical example and the corresponding relative error. Above: Reference and initial log-permeability field. Middle: Numerical approximation of the log-permeability field using LM and SVD algorithms. Bottom: Relative error in the estimation of the permeability field using LM and SVD algorithms. The relative error for each field is calculated by dividing the absolute error by the modulus of the reference value.

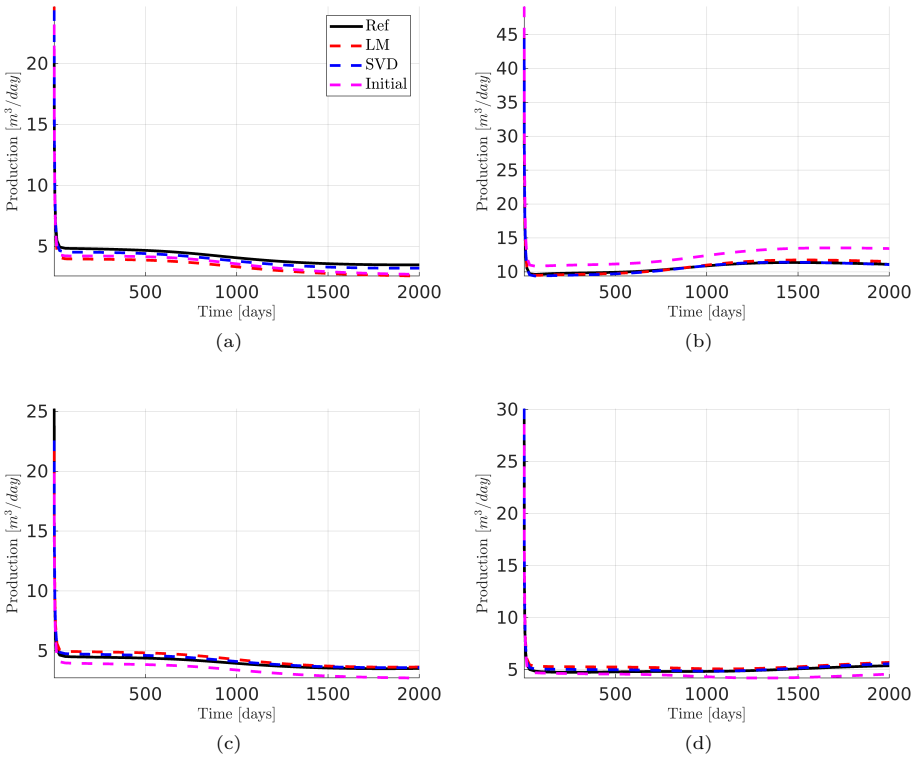


Fig. 5: Numerical Model: noisy numerical production rate of the SP10 model after contaminated with 2% RGN. Production rates of the water production rate versus time, associated with production wells W_1 (a), W_2 (b), W_3 (c) and W_4 (d). Solid lines denote the reference solution and dashed line the initial, optimal approximation from LM and SVD.

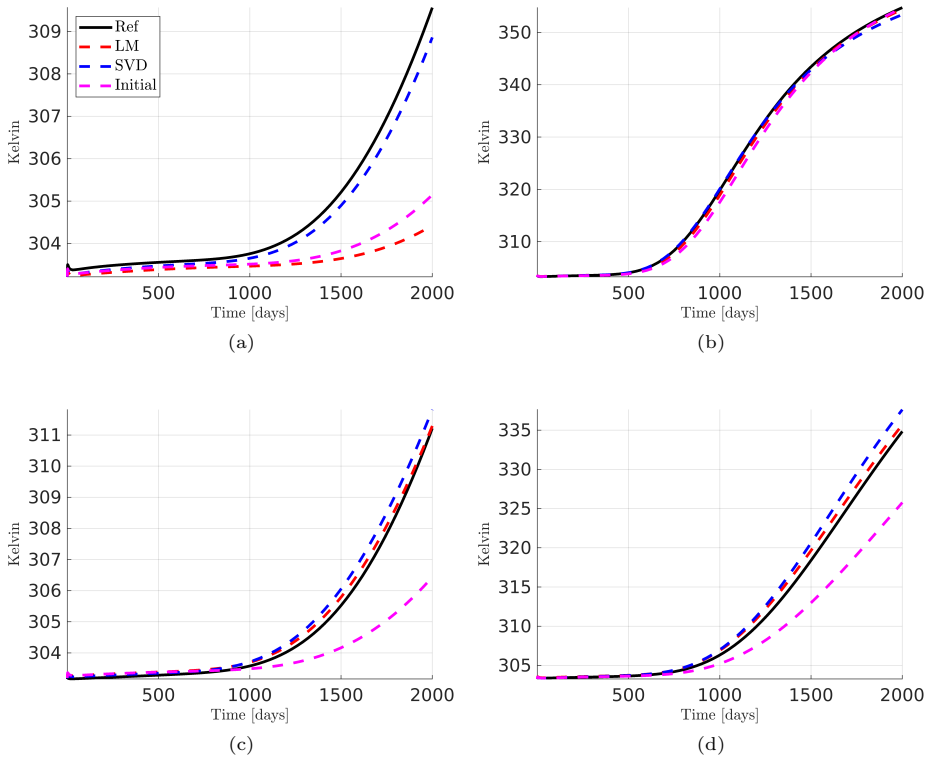
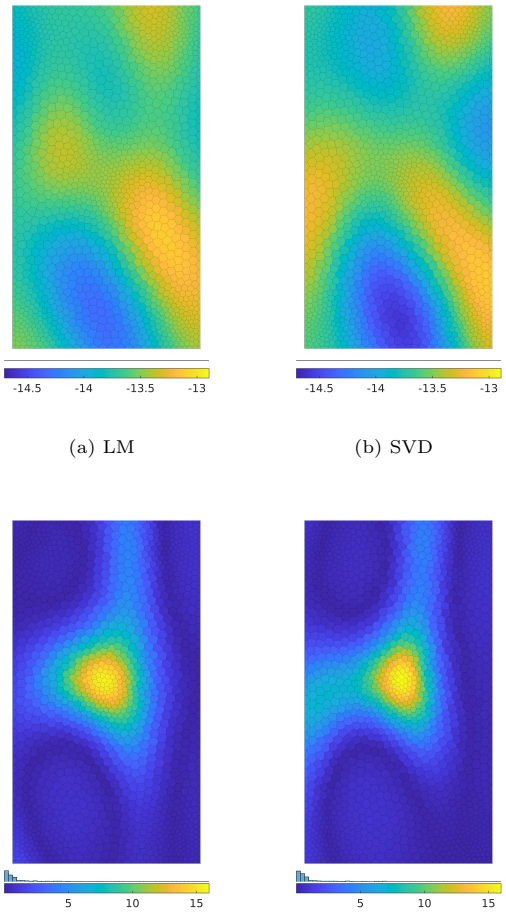


Fig. 6: Numerical Model: noisy numerical temperature of the SP10 model after contaminated with 2% RGN. Temperature versus time, associated with production wells W_1 (a), W_2 (b), W_3 (c) and W_4 (d). Solid lines denote the reference solution and dashed line the initial, optimal approximation from LM and SVD.



(a) LM (b) SVD

(c) LM (d) SVD

Fig. 7: Recovered fields of the 2% noisy numerical example and the corresponding relative error. Above: Numerical approximation of the log-permeability field using LM and SVD algorithms. Bottom: Relative error in the estimation of the permeability field using LM and SVD algorithms. The relative error for each field is calculated by dividing the absolute error by the modulus of the reference value.

8 Discussion

The numerical results using the SPE 10 model demonstrate the effectiveness of both the LM and SVD based inverse approaches for reconstructing the permeability field in a complex heterogeneous reservoir. The Gaussian covariance structure, combined with the truncated Karhunen-Loève expansion using only the first $M = 20$ dominant modes, captured over 95% of the total variance, ensuring a compact yet accurate representation of the uncertain parameter space.

Both LM and SVD algorithms successfully reduced the misfit function in the noise-free case: the LM method achieved a final misfit of 0.01147 after 100 iterations, while the SVD method reached 0.03147 in just 30 iterations. Although the LM algorithm yielded a more accurate match to the reference data, the SVD approach required significantly fewer iterations, highlighting its computational efficiency.

Figures 2 and 3 confirm that the optimized models from both methods closely reproduce the reference pressure and temperature profiles at all four production wells. Moreover, the reconstructed permeability fields in Figure 4 show substantial improvements over the initial guess. The LM reconstruction provides a more detailed approximation of the true log-permeability field, albeit at a higher computational cost.

In the presence of 2% synthetic noise in the well log data, the SVD inversion showed comparatively better robustness, achieving a superior fit than the LM approach under perturbed conditions. This suggests that the SVD method may offer enhanced performance in practical applications involving measurement uncertainty or incomplete information.

9 Conclusions

In this study, we combined the LM and SVD algorithms with the conditional Karhunen-Loève expansion to compute the inversion of permeability fields in heterogeneous porous media. The coefficients of the cKLE depend on production well data that are used to obtain the minimum misfit.

The application of the LM and SVD algorithms in cKLE allowed the optimization of coefficients in the KLE in complex geothermal models, contributing to a better characterization of geothermal reservoirs. In our approach, KLEs are constructed using the eigendecomposition of covariance models of spatial variability. Thus, we need to compute the eigenfunctions only once in the process of parameterizing the fields, which represents an advantage in the computational cost of inversion.

Through the KLE, we were able to present a methodology to reduce the dimension of the spatial mesh in parameterizing permeability fields while retaining a desired level of variance. If the entire field dimension were considered, the inversion process would involve extensive direct simulations in computing the Jacobian matrix. In our case, the dimension associated with parameterization was reduced from $M = 2500$ to $M = 20$ in the SPE 10 model. This drastically reduced the calculation of the Jacobian matrix in the LM and SVD algorithms.

Additionally, these algorithms converged accurately to the target field when applied to noise-free data. Notably, the SVD algorithm required 30 iterations to achieve convergence, however, the misfit result was higher than the LM. We then introduce a

2% noise level in the fitting process between the acquired and computed data in well logs. In this case, the inversion of permeability fields based on SVD demonstrated a comparatively superior fit compared to the LM-based approach.

Declarations

Ethics approval and consent to participate

This study did not involve human participants or animals, and thus ethics approval and consent to participate are not applicable.

Consent for publication

This manuscript does not include any individual person's data in any form, and thus consent for publication is not applicable.

Funding

This research was supported by National Council for Scientific and Technological Development (CNPq) - Brazil (Projects 406703/2023-0, 406477/2022-1, 402377/2022-2), Foundation for Research and Innovation Support of the State of Santa Catarina (FAPESC) (Project 00001993/2024) and Biocal Burntech.

Data availability

The authors declare that the data and codes supporting the findings of this study will be available as supplementary files in the online version of the paper, once the article is accepted.

Competing interests

The authors declare that they have no competing interests.

Authors' contributions

Juarez S. Azevedo: Conceptualization, funding acquisition, investigation, methodology, project administration, writing-original draft. Jarbas A. Fernandes: Writing. Marcus V. Americano da Costa: writing.

Acknowledgements

This declaration is not applicable.

References

[1] Rahmouni, S., Settou, N., Chennouf, N., Negrou, B., Houari, M.: A technical, economic and environmental analysis of combining geothermal energy with carbon sequestration for hydrogen production. Energy Procedia **50**, 263–269 (2014)

[2] Sakhaee-Pour, A.: Pore-scale modeling of the geysers. Geothermics **60**, 58–65 (2016)

[3] Azevedo, J.S., Murad, M.A., Borges, M.R., Oliveira, S.P.: A space–time multiscale method for computing statistical moments in strongly heterogeneous poroelastic media of evolving scales. International Journal for Numerical Methods in Engineering **90**(6), 671–706 (2012)

[4] Artus, V., Furtado, F., Noetinger, B., Pereira, F.: Stochastic analysis of two-phase immiscible flow in stratified porous media. Computational & Applied Mathematics **23**(2-3), 153–172 (2004)

[5] Borges, M.R., Pereira, F.: A novel approach for subsurface characterization of coupled fluid flow and geomechanical deformation: the case of slightly compressible flows. Computational Geosciences **24**(4), 1693–1706 (2020)

[6] Ginting, V., Pereira, F., Rahunanthan, A.: Multiple Markov chains Monte Carlo approach for flow forecasting in porous media. Procedia Computer Science **9**, 707–716 (2012)

[7] Park, H.M., Cho, D.H.: The use of the Karhunen-Loeve decomposition for the modeling of distributed parameter systems. Chemical Engineering Science **51**(1), 81–98 (1996)

[8] Gavin, H.P.: The Levenberg-Marquardt algorithm for nonlinear least squares curve-fitting problems. Department of civil and environmental engineering, Duke University **19** (2019)

[9] Yamashita, N., Fukushima, M.: On the rate of convergence of the Levenberg-Marquardt method. In: Topics in Numerical Analysis: With Special Emphasis on Nonlinear Problems, pp. 239–249 (2001). https://doi.org/10.1007/978-3-7091-6217-0_18 . Springer

[10] Gomaa, A.M.M., Péter, S.N., Mihály, D.: Petrophysical parameters estimation using Levenberg-Marquardt and Singular Value Decomposition inversion schemes. Multidiszciplináris Tudományok **11**(5), 24–38 (2021)

[11] Xu, P.: Truncated SVD methods for discrete linear ill-posed problems. Geophysical Journal International **135**(2), 505–514 (1998)

[12] Li, J., Tartakovsky, A.M.: Gaussian process regression and conditional Karhunen-Loève expansion for forward uncertainty quantification and inverse modeling in the presence of measurement noise. Journal of Machine Learning for Modeling and Computing **3**(2) (2022)

[13] Li, J., Tartakovsky, A.M.: Physics-informed karhunen-loéve and neural network approximations for solving inverse differential equation problems. Journal of

Computational Physics **462**, 111230 (2022)

[14] Tartakovsky, A.M., Barajas-Solano, D.A., He, Q.: Physics-informed machine learning with conditional Karhunen-Loève expansions. Journal of Computational Physics **426**, 109904 (2021)

[15] Yeung, Y.-H., Barajas-Solano, D.A., Tartakovsky, A.M.: Gaussian process regression and conditional Karhunen-Loève models for data assimilation in inverse problems. Journal of Computational Physics **502**, 112788 (2024)

[16] Chang, H., Zhang, D.: Jointly updating the mean size and spatial distribution of facies in reservoir history matching. Computational Geosciences **19**, 727–746 (2015)

[17] Møyner, O., Lie, K.A.: Advanced Modeling with the MATLAB Reservoir Simulation Toolbox (MRST) (2021)

[18] Lie, K.-A.: An Introduction to Reservoir Simulation Using MATLAB/GNU Octave: User Guide for the MATLAB Reservoir Simulation Toolbox (MRST). Cambridge University Press, ??? (2019)

[19] Azevedo, J.S., Fernandes, J.A.: The parameter inversion in coupled geomechanics and flow simulations using Bayesian inference. Journal of Computational Mathematics and Data Science **9**, 100083 (2023)

[20] Azevedo, J.S., Cardoso, G.S., Schnitman, L.: An adaptive Monte Carlo Markov Chain method applied to the flow involving self-similar processes in porous media. Journal of Porous Media **17**(3) (2014)

[21] Zhang, D., Lu, Z.: An efficient, high-order perturbation approach for flow in random porous media via Karhunen–Loeve and polynomial expansions. Journal of Computational Physics **194**(2), 773–794 (2004)

[22] Shinozuka, M.: Simulation of multivariate and multidimensional random processes. The Journal of the Acoustical Society of America **49**(1B), 357–368 (1971)

[23] Davis, M.W.: Production of conditional simulations via the LU triangular decomposition of the covariance matrix. Mathematical geology **19**, 91–98 (1987)

[24] Beaudoin, A., De Dreuzy, J.-R., Erhel, J., Pichot, G.: Convergence analysis of macro spreading in 3D heterogeneous porous media. In: ESAIM: Proceedings, vol. 41, pp. 59–76 (2013). EDP Sciences

[25] Dimitrakopoulos, R., Luo, X.: Generalized sequential Gaussian simulation on group size ν and screen-effect approximations for large field simulations. Mathematical geology **36**, 567–591 (2004)

[26] Krogstad, S., Lie, K.-A., Møyner, O., Nilsen, H.M., Raynaud, X., Skaflestad, B.: Mrst-ad–an open-source framework for rapid prototyping and evaluation of reservoir simulation problems. In: SPE Reservoir Simulation Symposium (2015). Society of Petroleum Engineers

[27] Azevedo, J.S.: Quasi Monte Carlo methods applied to equations in transient regime on the Theis equation. Monte Carlo Methods and Applications **18**(3), 201–216 (2012)

[28] Azevedo, J.S., Oliveira, S.P.: A numerical comparison between quasi-Monte Carlo and sparse grid stochastic collocation methods. Communications in Computational Physics **12**, 1051–1069 (2012)

[29] Oliveira, S.P., Azevedo, J.S.: Spectral element approximation of Fredholm integral eigenvalue problems. Journal of Computational and Applied Mathematics **257**, 46–56 (2014)